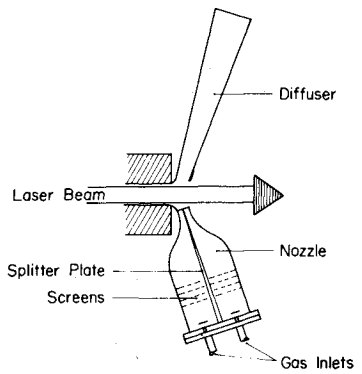

Fig. 1 Schematic diagram of the free-vortex aerowindow.

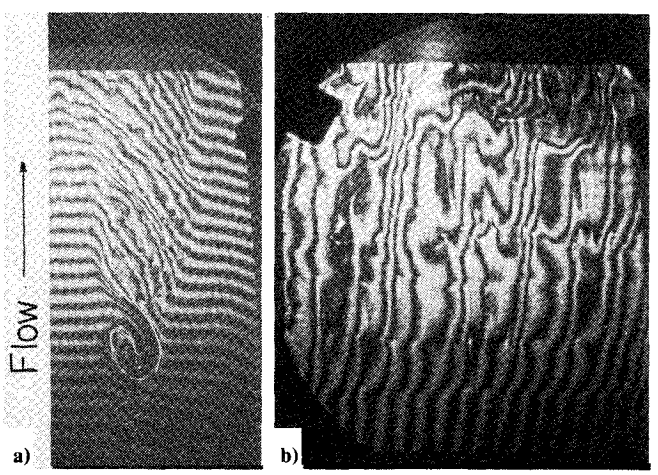

Fig. 2 Interferograms of the conventional free-vortex subsonic aerowindow flow: a) view of the turbulent interface; b) view through the turbulent interface.

high-pressure gas storage reservoir, the inner jet with a gas mixture of Ar:He:N_2 in the ratio 5:4:1 ($\beta = 2\times10^{-4}$) matched to the index of the CO_2 laser, and the outer jet with nitrogen ($\beta = 3\times10^{-4}$). The gas is introduced into each chamber through sonic orifices located at the bottom of the outlet. Splash plates disperse the orifice flow, and a series of four screens located downstream serve to smooth out the flow in the inlet before the jets emerge from the nozzle.

Diagnostics in this study consisted of a hot-wire anemometer utilized for flowfield surveys, and a Mach-Zender interferometer used to study the optical medium homogeneity of the aerowindow flow.

Interferograms of the free-vortex aerowindow operating in a conventional mode with both jets discharging the aerowindow gas mixture (5:4:1), where the index of refraction discontinuity occurs at the turbulent free-shear layer, are shown in Fig. 2. Figure 2a reveals the characteristics of the mixing zone by "looking" with the interferometer parallel to the turbulent interface, and Fig. 2b shows an interferogram "looking" through the turbulent interface. In the former, we notice the vortical structure close to the jet exit which disintegrates further downstream along the mixing zone. Figure 2b shows the large optical distortions introduced into the flow by the large index fluctuations at the free-shear layer. The fringe structure in this picture also reveals the vortical structure of the shear layer and the node points.

The significant reduction in the optical distortions achieved in the flow of the improved aerowindow is reflected in the interferogram shown in Fig. 3. Here the aerowindow gas mixture flows from the inner jet, and nitrogen flows from the outer jet. The index of refraction discontinuity is taken at a region where the two gases flow in parallel with identical velocity. Comparison with the no-flow reference interferogram shows that the fringes in Fig. 3 maintain the same structure with minimal large-scale distortions, indicating the high optical quality of the flow. The small-scale wake turbulence is reflected in the small wriggles superimposed on the fringes.

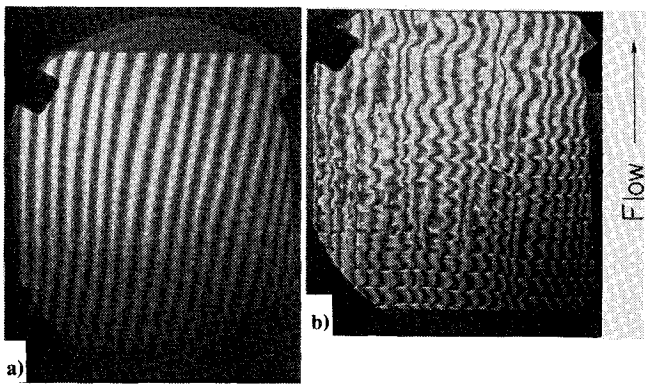

Fig. 3 Interferogram of the improved aerowindow flow: a) no flow; b) with flow.

Beam-direction interferograms, such as Figs. 2b and 3, were analyzed following the procedure outlined in Ref. 5. The results of this data analysis show the significant reduction in laser beam intensity losses in the improved aerowindow, with

$$\Delta I/I_o = 0.03$$

compared with 0.10 for the conventional-type aerowindow.

Acknowledgment

This work was supported by Office of Naval Research under Contract No. N00014-72-C-0276.

References

[1] Parmantier, E. M. and Greenberg, R. A. "Supersonic Flow Aerodynamic Windows for High-Power Lasers," *AIAA Journal*, Vol. 11, July 1973, pp. 943-949.

[2] Zimet, E., "Aerodynamic Windows for Laser Beams," NOLTR 73-66, Naval Ordance Laboratory, White Oak, Md., March 1973.

[3] Jones, T. G., "Development of an Aerodynamic Window," AFWL-TR-72-46, Air Force Weapons Laboratory, Albuquerque, N.M., July 1972.

[4] Sutton, G. W., "Effect of Turbulent Fluctuations in a Optically Active Medium," *AIAA Journal* Vol. 7, Sept. 1969, pp. 1737-1746.

[5] Legner, H. H., Otis, J. H., Theophanis, G. A., and Feinberg, R. M., "Laser Beam Degradation Through Turbulent Interfaces," AIAA Paper 78-71, Huntsville, Ala., 1978.

Effect of Suction on a Shock-Separated Boundary Layer—A Numerical Study

Y. Tassa* and N. L. Sankar†
Lockheed-Georgia Company, Marietta, Ga.

I. Introduction

THE performance of many aerodynamic components at transonic and supersonic flight conditions is adversely affected by the interaction of external shocks with the boundary layer. If the shock wave is sufficiently strong, the

Received May 7, 1979.

Index categories: Jets, Wakes, and Viscid-Inviscid Flow Interactions; Shock Waves and Detonations; Computational Methods.

*Research Scientist. Member AIAA.
†Scientist Associate. Member AIAA.

boundary layer will separate. It is, therefore, of interest to eliminate or control these adverse effects (thickening of the boundary layer, onset of transition, separation, etc.) through suitable boundary-layer control techniques such as suction, blowing, or cooling of walls. In the present study, the compressible Navier-Stokes equations are solved numerically to study boundary-layer control through suction.

II. Analysis

The two-dimensional, unsteady Navier-Stokes equations in Cartesian coordinates written in the conservative law form are:

$$\frac{\partial U}{\partial t}+\frac{\partial F}{\partial x}+\frac{\partial G}{\partial y}=0 \tag{1}$$

where

$$U=\begin{vmatrix}\rho\\ \rho u\\ \rho v\\ \rho E\end{vmatrix} \qquad F=\begin{vmatrix}\rho u\\ \rho u^2+\sigma_x\\ \rho uv+\tau_{xy}\\ \rho uE+u\sigma_x+v\tau_{xy}+q_x\end{vmatrix}$$

and

$$G=\begin{vmatrix}\rho v\\ \rho uv+\tau_{xy}\\ \rho v^2+\sigma_y\\ \rho vE+u\tau_{xy}+v\sigma_y+q_y\end{vmatrix}$$

where ρ, u, v, and E are the density, velocity components, and total specific energy, respectively. The stress tensor components σ_x, σ_y, and τ_{xy} are known for a Newtonian fluid. The heat flux quantities q_x and q_y are related to temperature gradients in the flowfield. The equation of state and a proper set of initial and boundary conditions are sufficient to obtain a closed system.

The numerical solution of Eq. (1) involves time linearization of the nonlinear terms and spatial factorization. These procedures are well-documented in the literature.[1,2] The version of the ADI factorization scheme used in the present code is second-order accurate in time and space.

Typical features of the physical flow problem are shown in Fig. 1. The computational grid for the problem is shown in Fig. 2. The grid points were spaced uniformly in the x direction and stretched in the y direction as follows:

$$\Delta Y=\Delta Y_{\text{out}}[\Delta Y_{\text{in}}/\Delta Y_{\text{out}}]^{(J_{\text{in}}-J)/J_{\text{in}}} \qquad 1\le J\le J_{\text{in}}$$

$$\Delta Y=\Delta Y_{\text{out}} \qquad J_{\text{in}}<J\le J_{\max}$$

For the present study,

$$I_{\max}=32,\ J_{\max}=45,\ J_{\text{in}}=33,$$

$$\Delta Y_{\text{in}}=0.00305 \text{ cm},\ \Delta Y_{\text{out}}=0.1948 \text{ cm}$$

The boundary conditions were specified as follows (see Fig. 2): Along line a-f the freestream conditions prevail. On the upper boundary, along f-e, the freestream conditions were specified. Along e-d, the postshock conditions were specified. At the downstream boundary c-d the flow properties were determined by two-point extrapolation. Along a-b, symmetry conditions were imposed using a three-point, one-sided difference scheme. On the solid wall, the x component of the velocity was set at zero; the y component of the velocity was specified depending on the amount of suction.

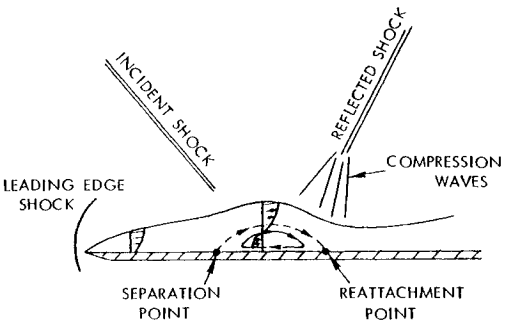

Fig. 1 Sketch of shock boundary-layer interaction.

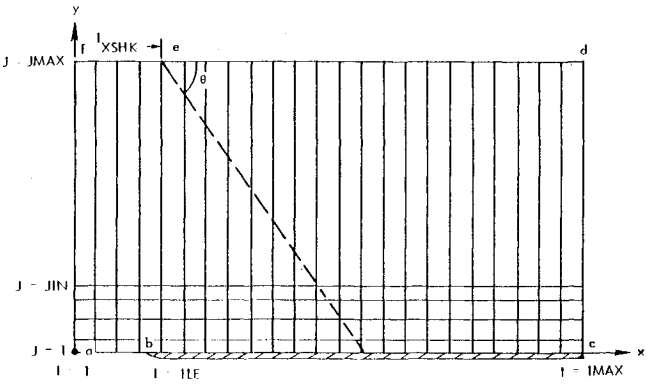

Fig. 2 Shock boundary-layer computational plane.

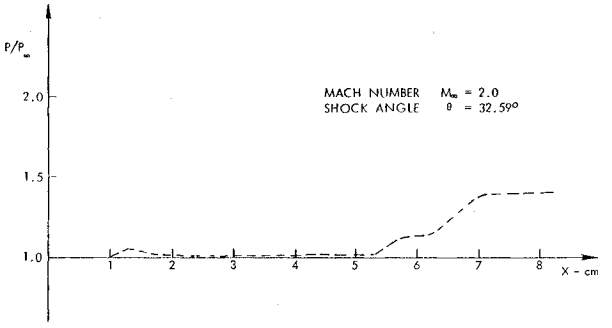

Fig. 3 Surface pressure distribution.

The adiabatic wall condition was invoked. While the density at the wall may be determined in a number of ways, a simple three-point extrapolation from the interior nodes proved to be satisfactory.

III. Results and Discussion

Two test cases were first studied to establish the accuracy and reliability of the present code: a) freestream Mach number 2.0, shock angle of 31.347, deg and Reynolds number of 0.284×10^6 based on the distance of the shock from the leading edge; and b) freestream Mach number 2.0, shock angle of 32.585 deg, and Reynolds number of 0.296×10^6.

In Fig. 3, the pressure distribution along the plate at steady state is shown for case b. The results were found to be in very good agreement with other numerical results.[2,3] Uniform suction was subsequently applied for case b, which has a separation bubble.

In Fig. 4, the velocity profiles in the separation region for two different suction velocities are plotted and compared with the no-suction case. The velocity profiles downstream of the interaction region are fuller when the suction is applied. With relatively small amounts of suction, the separation region can be eliminated. Since the profiles are free of inflection points,

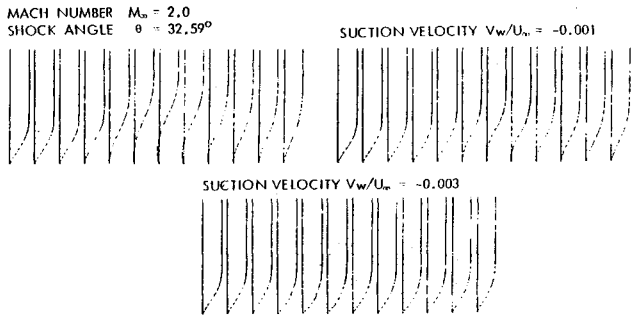

Fig. 4 Velocity profiles in the separated region.

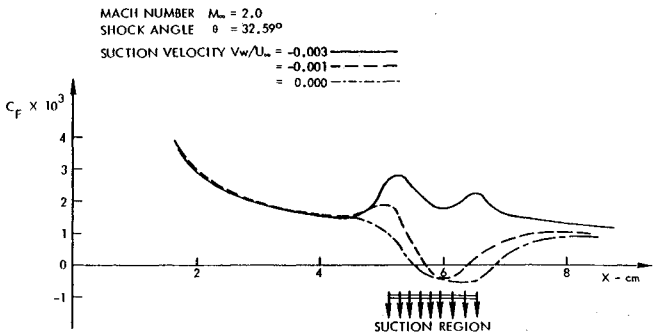

Fig. 5 Skin-friction coefficient distribution.

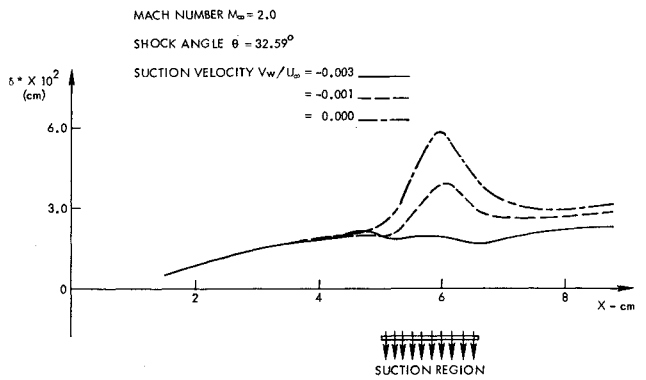

Fig. 6 Displacement thickness distribution.

suction contributes to the stability of the boundary layer. In Fig. 5 the skin-friction coefficient for the three cases are shown for comparison. The wavy nature of the skin-friction coefficient distribution is due to the counteracting effects of the shock adverse pressure gradient and suction. The displacement thickness distribution is plotted in Fig. 6. Even a modest amount of suction of about 0.3% of freestream velocity substantially reduces the boundary-layer thickness in the separation region.

The preceding computations, though preliminary in nature, allow us to predict the effect of suction quantitatively. Currently, investigations are under way to study shock-turbulent boundary-layer suction interaction problems. It is hoped that this work will act as a stepping stone in other important studies of boundary-layer control.

References

[1] Briley, W. R. and McDonald, H., "An Implicit Numerical Method for the Multidimensional Compressible Navier-Stokes Equations," United Aircraft Research Labs., Rept. M911363-6, 1973.

[2] Beam, R. and Warming, R. F., "An Implicit Factored Scheme for the Compressible Navier-Stokes Equations," AIAA Paper 77-645, June 1977.

[3] MacCormack, R. W. and Baldwin, B. S., "A Numerical Method for Solving the Navier-Stokes Equations with Application to Shock-Boundary Layer Interactions," AIAA Paper 75-1, Jan. 1975.

Location and Magnitude of Cascade Shock Loss by High-Speed Smoke Visualization

William B. Roberts*
Nielsen Engineering & Research, Inc., Mountain View, Calif.
and John A. Slovisky†
University of Notre Dame, Notre Dame, Ind.

Introduction

INVESTIGATING the flowfield in a real transonic flow poses several challenges. The use of any type of intrusive probe will not only seriously affect any shock present in the flow but can produce an interfering shock pattern of its own. Also, near a Mach number of one, the flow is extremely sensitive to any area change due to blockage effects. For these reasons, a method that allows quantitative data acquisition without the use of instrusive probes is highly desirable. The high-speed flow visualization technique under development at the University of Notre Dame is such a method, making it possible to determine quantitative data on shock strength and location through a combination of shadowgraph and smoke flow photographs.

The inviscid compressible flow theory predicts a deflection of streamlines passing an oblique or curved shock.[1] The local inclination of the shock to the upstream direction, together with the deflection of the streamline through the shock, can be used to determine the upstream and downstream Mach numbers across the shock. The pertinent relationships from the compressible flow theory are:

$$\tan\theta = 2\cot\psi\left[\frac{M_1^2\sin^2\psi - 1}{M_1^2(k+\cos 2\psi)+2}\right] \tag{1}$$

$$M_2^2\sin^2(\psi-\theta) = \frac{1+\left(\frac{k-1}{2}\right)M_1^2\sin^2\psi}{kM_1^2\sin^2\psi - \left(\frac{k-1}{2}\right)} \tag{2}$$

where: M_1 and M_2 = upstream and downstream Mach number respectively; ψ = local inclination angle of shock with upstream flow; θ = streamline deflection through shock wave; and k = ratio of specific heat. They are illustrated in Fig. 1. If the local shock inclination ψ, together with the deflection θ, along streamlines could be determined along a shock wave, then the upstream and downstream Mach numbers could be calculated and the shock pressure ratio and loss determined.

Test Equipment and Procedure

All testing was done in the Planar High-Speed Smoke Tunnel (PHSST) at the Aerospace Laboratory of the University of Notre Dame. A complete description and drawings of the PHSST are given in Refs. 2 and 3. The

Presented as Paper 79-0042 at the AIAA 17th Aerospace Sciences Meeting, New Orleans, La., Jan. 15-17, 1979; submitted Jan. 31, 1979; revision received June 22, 1979.

Index categories: Transonic Flow; Nozzle and Channel Flow; Airbreathing Propulsion.

*Project Engineer. Member AIAA.
†Research Assistant, Dept. of Aerospace and Mechanical Engineering. Member AIAA.